Vision-Based Material Tracking in Heavy-Plate Rolling

Automation and Control Institute (ACIN)
TU Wien
Gusshausstrasse 27-29/E376
1040 Vienna, Austria

Internet: www.acin.tuwien.ac.at
E-mail: office@acin.tuwien.ac.at
Phone: +43 1 58801 37601
Fax: +43 1 58801 37699

Vision-Based Material Tracking in Heavy-Plate Rolling

Florian Schausberger * **Andreas Steinboeck** * **Andreas Kugi** *
Martin Jochum ** **Daniel Wild** ** **Thomas Kiefer** **

* *Automation and Control Institute, TU Wien, Vienna, Austria (e-mail: {schausberger, steinboeck, kugi}@acin.tuwien.ac.at)*
** *AG der Dillinger Hüttenwerke, Dillingen, Germany (e-mail: {martin.jochum, daniel.wild, thomas.kiefer}@dillinger.biz)*

Abstract: Knowledge of the position and the material conditions, e.g. the temperature, of the plates during hot rolling is important for process control. In fact, a precise material tracking system may help to prevent problems during the production process. This paper deals with the tracking of the rotation of heavy plates before and after the lateral expansion phase. The presented approach estimates the orientation and the position of the plate moving on the roller table. Images captured by a thermographic camera are utilized to identify the edges of the plate within the field of view. The detected edges are fed into an optimization-based estimation of the angular and translational position of the plate. Measurements of a plate from an industrial rolling mill demonstrate that the proposed method is robust against disturbances from the harsh environment nearby the mill stand.

Keywords: Hot rolling, material tracking, image processing, thermographic imaging, edge detection, unconstrained optimization

1. INTRODUCTION

The considered rolling mill of AG der Dillinger Hüttenwerke, Germany, is outlined in Fig. 1. The slabs are first reheated in one of the furnaces. During the heating process, a scale layer builds up, which is removed in a descaling unit before the actual rolling steps at the roughing mill. After the beginning of the rolling process, the product is called plate. Following the lateral expansion to the desired width at the roughing mill, the plate is rolled in longitudinal direction to the desired plate thickness and length at the finishing mill. In the following cooling section, a specific reduction of the plate temperature may be enforced to obtain the desired mechanical properties of the plate material. Then, the plate is leveled to reduce residual stresses.

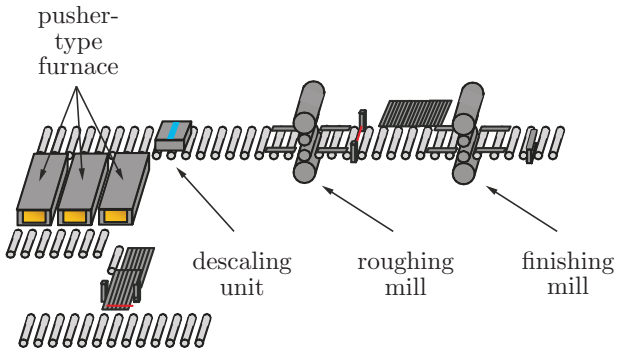

Fig. 1. Processing line of AG der Dillinger Hüttenwerke, Germany.

The temperature of the plate undergoes large changes during the production process. Since the temperature evolution is significant for the properties of the final product, it has to be carefully considered when planning the roll pass schedule. A large-area roller table is located between the roughing mill and the finishing mill. It is used to store plates until they have reached the necessary temperature for the subsequent processing at the finishing mill. The cooling time of a specific plate on the large-area roller table depends on the processed type of steel and the performed metallurgic treatments. Several plates with varying material properties and dimensions are simultaneously processed in this production line. Because different cooling times may be needed, the processing order of the plates can change during the production. Clearly, a precise tracking of the plate position is necessary to distinguish between the plates.

A vision-based material tracking approach in heavy plate rolling was proposed by Tratnig et al. (2007). They used 4 visible light cameras with overlapping fields of view to track the position of the plates between a descaler and a rolling mill. Vision-based systems are also used for material tracking during the rolling pass itself, see, e.g., (González et al., 2001; Montague et al., 2005; Carruthers-Watt et al., 2010; Schausberger et al., 2015).

Contrary, this paper deals with a special part of the whole material tracking problem. After the heating and the descaling of the slabs, they are first rolled in width direction to their desired plate width. In the subsequent rolling passes, the plate is rolled in longitudinal direction to its final plate length. Before and after the lateral expansion, the slabs or plates have to be rotated with

Post-print version of the article: F. Schausberger, A. Steinboeck, A. Kugi, M. Jochum, D. Wild, and T. Kiefer, "Vision-based material tracking in heavy-plate rolling", in *Proceedings of the 17th IFAC Symposium on Control, Optimization and Automation in Mining, Mineral and Metal Processing (MMM)*, vol. 49, Vienna, Austria, 2016, pp. 108–113. DOI: 10.1016/j.ifacol.2016.10.105

respect to their vertical axis, i.e., at least 2 rotations of the plate are necessary. The rotation in front of the mill stand is performed by means of a roller table with tapered rolls. Here, the tapering of the rolls is alternately arranged (cf. Fig. 2). This special type of roller table has two roller pairs which can be individually rotated.

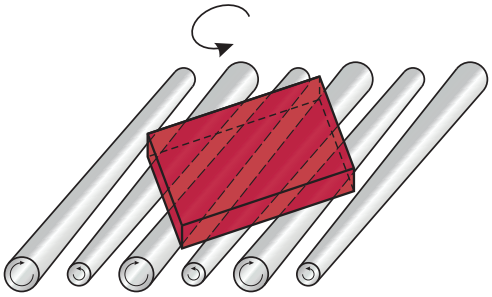

Fig. 2. Roller table with tapered rolls and rotating plate.

The rotation of the plate is currently controlled by the mill stand operator. However, feedback control could help to reduce the time needed for the rotation of the plate and hence may yield considerable time savings during the rolling process. A simple feedforward control of the plate rotation is not possible due to the slip between the plate and the rolls of the roller table. Hence, feedback control should be applied to control the rotation of the plate which essentially builds up on the knowledge of the angular position of the plate. In this work, a method to estimate the angular position is presented.

The paper is organized as follows: An infrared camera mounted at the ceiling of the rolling-mill building captures images of the plate lying on the roller table. Within the infrared bitmaps, a threshold based edge detection is performed which is discussed in Section 2. The detected edges are then used in Section 3 in an optimization-based approach to estimate the plate movement. Measurements of a plate taken from the standard production process are presented in Section 4 to prove the feasibility of the proposed method. Section 5 contains a short summary and gives an outlook on further research activities.

A more detailed description of the calculation steps of the presented material tracking approach is given in Tab. 1.

2. EDGE DETECTION

The first step of the presented material tracking approach is the detection of the plate edges within the images captured by an infrared 2D-CCD camera. Compared to standard cameras for visible light, infrared cameras are superior for the considered application due to the following properties:

- Objects can be captured through a cloud of steam.
- The thermal contrast between the plate and its environment is high and therefore no illumination is needed.
- There is no disturbance of the images due to other light sources, e.g. sunlight.

The first property is beneficial for the subsequent edge detection because the plate may be surrounded by a cloud of steam due to the cooling water sprayed onto the plate during the rolling process. Furthermore, the high thermal contrast (cf. Fig. 3) enables a simple threshold-based edge detection. Clearly, visible light cameras are suffering from disturbing light sources which may entail erroneously detected edges, see, e.g., (Montague et al., 2005). However, disturbing radiation sources are seldom in the measured infrared range of thermographic cameras. Additionally, the measured temperature distribution of the surface of the plate can be used for process monitoring and process control.

Table 1. Calculation steps of the material tracking approach and their results.

Step	Result
image capturing	monochrome bitmap of radiation intensity
edge pixel detection in rows and columns	edge pixels in vertical and horizontal direction
clustering of edge pixels	4 clusters of edge pixels representing the 4 plate edges
fitting of a polynomial to each cluster of the initial plate configuration	4 polynomials representing the plate edges of the initial configuration
solving of the optimization problem for the actual configuration	position and orientation of the plate

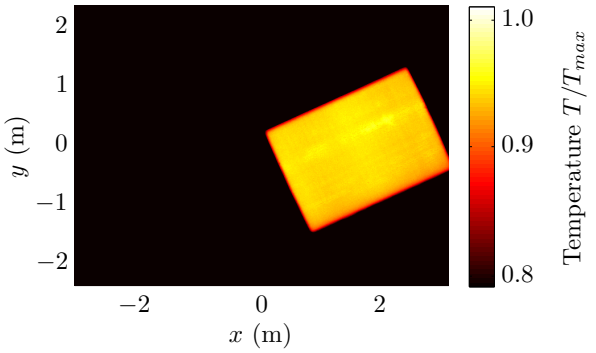

Fig. 3. Thermographic bitmap of a rotating heavy plate.

The camera is mounted 25 m above the pass level of the roller table. Mounting the camera at the ceiling of the rolling-mill building isolates the camera from vibrations, steam, and dust induced during the rolling pass and hence renders an air flushing of the lens of the camera unnecessary. The industrial camera captures 30 frames/s with an image resolution of 659×494 pixels. Using a 25 mm lens, a spatial resolution of approximately 1 cm/pixel is achieved. The origin of a fixed global coordinate frame (x, y, z) is located at the center of the field of view (FOV).

The camera is connected via Gigabit Ethernet to a PC and addressed using the so called pylon API. The pylon API is based on the GenICam standard and allows an interface-independent control of the camera in the respective software application. Furthermore, the pylon API allows to change a large number of parameters of the camera. An important parameter is the exposure time which has to be properly chosen to get high contrast images. The camera

Post-print version of the article: F. Schausberger, A. Steinboeck, A. Kugi, M. Jochum, D. Wild, and T. Kiefer, "Vision-based material tracking in heavy-plate rolling", in *Proceedings of the 17th IFAC Symposium on Control, Optimization and Automation in Mining, Mineral and Metal Processing (MMM)*, vol. 49, Vienna, Austria, 2016, pp. 108–113. DOI: 10.1016/j.ifacol.2016.10.105
The content of this post-print version is identical to the published paper but without the publisher's final layout or copy editing.

features an automatic control of the exposure time. Here, the exposure time is adjusted until an average intensity in a user-defined area of interest (AOI) is reached. In the considered application, this AOI is chosen inside the plate boundaries.

Several algorithms are available for the detection of edges in bitmaps. These algorithms differ in terms of accuracy and computational effort. A frequently used approach is the so called *Canny-algorithm* (cf. Canny, 1986). However, for the considered application, a tailored algorithm for the detection of the plate edges is used because it features a lower computational effort and simplifies the subsequent image processing steps. The pylon API provides the local intensity of the detected infrared radiation in the form of a monochrome bitmap with 12 bit resolution. Instead of the temperature bitmap, the intensity bitmap is utilized for detecting the edges. This is favorable because the intensity features similar transitions from the hot plate to the cold surrounding area even for different temperature levels, which simplifies the choice of an appropriate intensity threshold I_{th}. For the considered application, the choice

$$I_{th} = I_{min} + \Lambda\,(I_{max} - I_{min})$$

with the minimum I_{min} and the maximum I_{max} of the intensity I in the considered image proved useful. The relative threshold $\Lambda \in [0, 1]$ is a user-defined constant. In every column of the image, the two outermost pixels where the threshold I_{th} is exceeded determine the edges in horizontal direction. Analogously, edges in the vertical direction are found by processing the rows of the image.

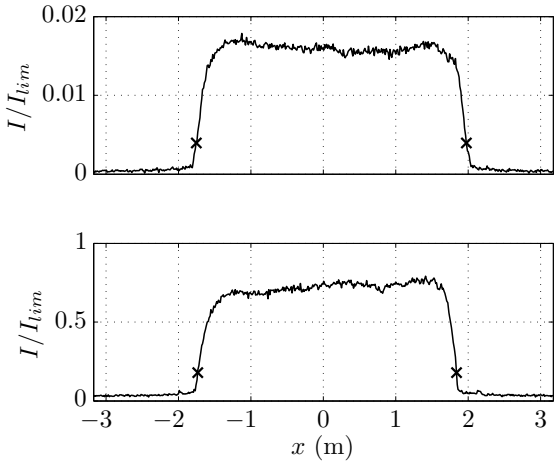

Fig. 4. Intensity distribution of a single row of a cold and a hot plate as well as detected edge pixels. The intensity is normalized to the upper measurement limit I_{lim} of the infrared camera.

Remark: The intensity is linked with the temperature by the Stefan-Boltzmann law $I = \sigma T^4$, where σ denotes the Stefan-Boltzmann constant (cf. Baehr and Stephan, 2006). Hence, an equivalent temperature threshold could alternatively be calculated and the edge pixel detection could be performed using the temperature bitmap. However, the relation between the intensity measured by the camera and the temperature deviates from Stefan-Boltzmann's law because of imperfections of the intensity measurement. The mapping used in the software of the camera is generally not open which denies a temperature based edge detection.

Fig. 4 shows the intensity distribution of a single row for two different plates. The upper part of Fig. 4 shows the intensity of a cold plate and in the lower part a very hot plate is shown. Both plates feature a steep slope from the outside margin of the plate to its inner part which turned out to be characteristic. The parameter Λ is chosen so that the detected edge pixels are in the region of the steep slope. The detected edge pixels for $\Lambda = 0.2$ are marked with crosses in Fig. 4.

After the threshold detection, the edge pixels are clustered into 4 edges of the plate. Fig. 5 shows the clustering for an exemplary plate. The left part of Fig. 5(a) shows the detected edge pixels in horizontal direction in red and blue dashed lines. Here, the edge pixels in horizontal direction

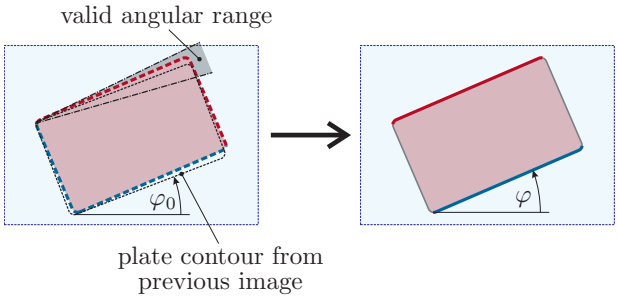

(a) Clustering of the horizontal edge pixels.

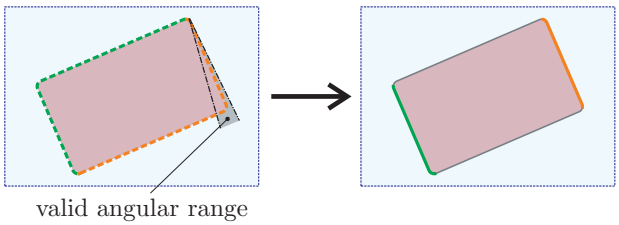

(b) Clustering of the vertical edge pixels.

Fig. 5. Clustering of the edge pixels into edges.

are used to extract the longitudinal edges as shown in the right part of Fig. 5(a). Consequently, the edge pixels in vertical direction are used to extract the lateral edges (cf. Fig. 5(b)).

The choice to use the horizontal edge pixels to extract the longitudinal edges and the vertical edge pixels to extract the lateral edges becomes obvious by considering Fig. 6. Here, the detected edge pixels are shown for simplicity reasons within a bitmap with a lower resolution than the used infrared bitmap. For the considered plate orientation, the number of edge pixels related to the longitudinal edges is larger when using the horizontal instead of the vertical

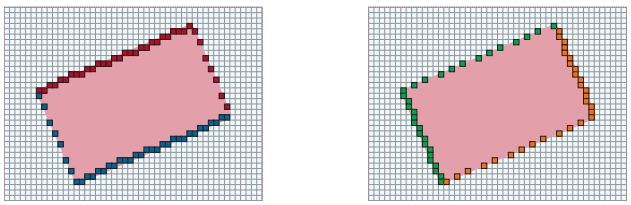

Fig. 6. Horizontal and vertical edge pixels in a bitmap with a low resolution.

Post-print version of the article: F. Schausberger, A. Steinboeck, A. Kugi, M. Jochum, D. Wild, and T. Kiefer, "Vision-based material tracking in heavy-plate rolling", in *Proceedings of the 17th IFAC Symposium on Control, Optimization and Automation in Mining, Mineral and Metal Processing (MMM)*, vol. 49, Vienna, Austria, 2016, pp. 108–113. DOI: 10.1016/j.ifacol.2016.10.105
The content of this post-print version is identical to the published paper but without the publisher's final layout or copy editing.

edge pixels. The same holds true for the lateral edges and the vertical edge pixels.

Clearly, the decision to choose the edge pixels in horizontal or in vertical direction for a specific plate edge relies on the orientation φ of the plate. However, the actual orientation φ is unknown during the edge detection and therefore the orientation φ_0 of the previously captured image is used. In particular, the horizontal edge pixels are clustered into longitudinal edges and the vertical edge pixels are clustered into lateral edges if $-\frac{\pi}{4} < \varphi_0 \leq \frac{\pi}{4}$ or $\frac{3\pi}{4} < \varphi_0 \leq \frac{5\pi}{4}$. For the remaining angular range, i.e., $\frac{\pi}{4} < \varphi_0 \leq \frac{3\pi}{4}$ or $\frac{5\pi}{4} < \varphi_0 \leq \frac{7\pi}{4}$, the vertical edge pixels are clustered into longitudinal edges and the horizontal edge pixels into lateral edges.

It is required that the angle φ of a valid edge is within a specific range, i.e.,

$$|\varphi - \varphi_0| < \gamma,$$

for at least K_{min} neighboring pixels with the angle φ_0 from the previously captured image and a constant $\gamma > 0$. The valid range is chosen based on the angular position of the plate estimated in the previously captured image. The local angle of the current edge is calculated using a Savitzky-Golay filter, see, e.g. (Orfanidis, 1996) with degree 2 and window length 11. The edges in the vertical direction of the image are processed in an analogous manner by filtering along the y-direction.

3. ESTIMATION OF THE ROTATION

In this section, an optimization-based approach for the estimation of the rotation of the plate is presented. It utilizes the plate edges found by the edge detection approach from Sec. 2. When the whole plate is inside the FOV of the camera for the first time, every edge of the plate is numbered (cf. Fig. 7) and parameterized by a polynomial

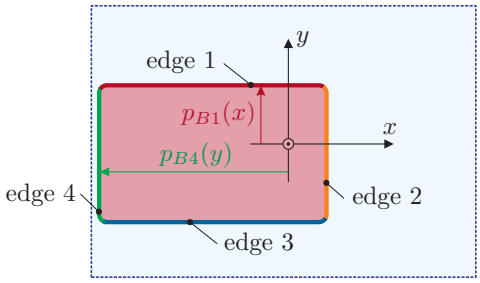

Fig. 7. Parameterization of the plate edges.

with degree N_B. This is called the initial configuration. The edges 1 and 3 of this initial configuration of the plate are parameterized as

$$p_{Bi}(x) = \sum_{j=0}^{N_B} d_{i,j} x^j, \quad i = 1, 3$$

and the edges 2 and 4 as

$$p_{Bi}(y) = \sum_{j=0}^{N_B} d_{i,j} y^j, \quad i = 2, 4.$$

Furthermore, a coordinate frame (x_{pl}, y_{pl}, z_{pl}) with base vectors $\mathbf{e}_{x_{pl}}$, $\mathbf{e}_{y_{pl}}$, and $\mathbf{e}_{z_{pl}}$ is fixed to the center of the plate as shown in Fig. 8. The origin of the plate-fixed coordinate frame at the time step k is shifted by $(\Delta x_k, \Delta y_k, 0)$ and rotated by the angle φ_k around the axis z with respect to the global coordinate frame. The initial configuration is characterized by x_0, y_0, and $\varphi_0 = 0$ rad.

The presented approach aims at minimizing the alignment error between the initial and the shifted actual configuration of the plate by an appropriate choice of the unknowns Δx_k, Δy_k, and φ_k. This idea is materialized in the static optimization problem

$$\begin{aligned} \min_{\Delta x_k,\, \Delta y_k,\, \varphi_k} \; & \sum_{j=1}^{N_{1,k}} \left(\bar{y}_{M1,j,k} - p_{B1}(\bar{x}_{M1,j,k})\right)^2 \\ & + \sum_{j=1}^{N_{2,k}} \left(\bar{x}_{M2,j,k} - p_{B2}(\bar{y}_{M2,j,k})\right)^2 \\ & + \sum_{j=1}^{N_{3,k}} \left(\bar{y}_{M3,j,k} - p_{B3}(\bar{x}_{M3,j,k})\right)^2 \\ & + \sum_{j=1}^{N_{4,k}} \left(\bar{x}_{M4,j,k} - p_{B4}(\bar{y}_{M4,j,k})\right)^2 \end{aligned} \tag{1a}$$

subject to

$$\begin{aligned} \begin{bmatrix} \bar{x}_{Mi,j,k} \\ \bar{y}_{Mi,j,k} \end{bmatrix} = & \begin{bmatrix} \cos(\varphi_k) & \sin(\varphi_k) \\ -\sin(\varphi_k) & \cos(\varphi_k) \end{bmatrix} \begin{bmatrix} x_{Mi,j,k} - \Delta x_k \\ y_{Mi,j,k} - \Delta y_k \end{bmatrix} \\ & + \begin{bmatrix} \Delta x_0 \\ \Delta y_0 \end{bmatrix} \end{aligned} \tag{1b}$$

using measurement pairs $(x_{Mi,j,k}, y_{Mi,j,k})$, $i = 1, \ldots, 4$. These pairs contain the spatial coordinates of the edge pixels detected in Sec. 2. Hence, $N_{i,k}$ denotes the number of detected edge pixels associated with the i-th edge at the time step k. The expression (1b) transforms these coordinates so that the plate-fixed coordinate frame coincides with the coordinate frame in the initial configuration. Each individual sum in (1a) penalizes the deviation between the polynomial representation and the measurements of a single edge. Note that the deviations are measured in the global coordinate frame (x, y, z) in y-direction for the transformed edges 1 and 3 and in x-direction for the transformed edges 2 and 4.

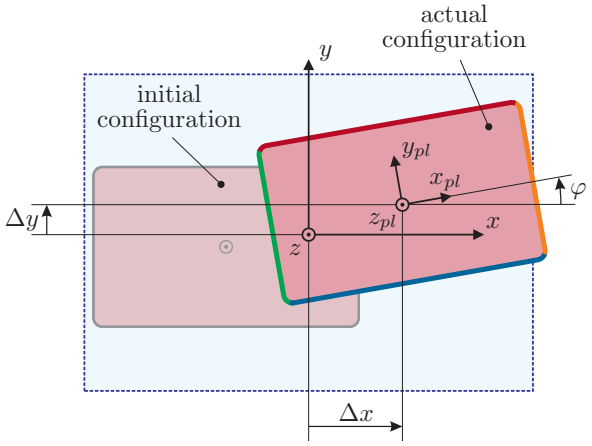

Fig. 8. Parameterization of the position and the orientation of the plate.

Post-print version of the article: F. Schausberger, A. Steinboeck, A. Kugi, M. Jochum, D. Wild, and T. Kiefer, "Vision-based material tracking in heavy-plate rolling", in *Proceedings of the 17th IFAC Symposium on Control, Optimization and Automation in Mining, Mineral and Metal Processing (MMM)*, vol. 49, Vienna, Austria, 2016, pp. 108–113. DOI: 10.1016/j.ifacol.2016.10.105
The content of this post-print version is identical to the published paper but without the publisher's final layout or copy editing.

The literature offers different algorithms for solving the optimization problem (1), see, e.g., (Nocedal and Wright, 2006) for an overview. For a compact notation, the normalized optimization variables are arranged in the vector $\mathbf{w} = [\Delta x_k/\mathrm{m}\ \Delta y_k/\mathrm{m}\ \varphi_k/\mathrm{rad}]^\mathrm{T}$. The objective function (1a) may be written in the quadratic form $J = \mathbf{e}^\mathrm{T}\mathbf{e}$. This property enables the use of the Gauss-Newton method, a numerical method to solve unconstrained optimization problems. It proved useful for the considered problem due its superlinear convergence rate and the fact that it only requires the evaluation of the Jacobian $\mathbf{J}$ of $\mathbf{e}$ with respect to $\mathbf{w}$ in every iteration but not the Hessian matrix. According to Nocedal and Wright (2006), the Gauss-Newton method proceeds as follows:

Step 0: Set the initial guess for $\mathbf{w}$.

Step 1: Compute the search direction $\mathbf{d} = -\left(\mathbf{J}^\mathrm{T}\mathbf{J}\right)^{-1}\mathbf{J}^\mathrm{T}\mathbf{e}$ with $\mathbf{J}(\mathbf{w}) = (\nabla\mathbf{e})^\mathrm{T}$.

Step 2: Perform the update $\mathbf{w} \leftarrow \mathbf{w} + \mathbf{d}$.

Step 3: Check if any termination criterion (maximum number of iterations, convergence) is fulfilled. If yes, stop here.

Step 4: Start again at Step 1.

The termination criterion $\|\mathbf{d}\|_\infty < \delta$ with the positive constant δ is used to check if the solution is acceptable. Furthermore, the Jacobian is calculated analytically which leads to a better convergence rate of the optimization problem compared to the use of numerical differentiation. The solution of the optimization problem at the time step k is used as initial guess for the subsequent optimization at the time step $k+1$.

4. MEASUREMENTS

In the following, results for a plate rolled at the heavy-plate mill of AG der Dillinger Hüttenwerke are presented. The results for the considered plate with 2.7 m length and 1.9 m width are shown in Fig. 9. The plate is first rotated using the roller table. The subsequent alignment of the plate in rolling direction is performed by maneuverable side guides of the rolling mill. The parameters used in the computations are listed in Tab. 2.

Table 2. Parameters of the material tracking problem.

Parameter	Value	Unit
Λ	0.2	
γ	0.7	rad
K_{min}	30	
N_B	2	
δ	10^{-3}	

In Fig. 9(a), the image of the plate captured at different time steps is shown for a time interval of 14 s. Furthermore, the edges detected with the approach from Sec. 2 are shown as green lines and the origin of the plate-fixed coordinate frame is marked with a red circle. As seen in the images of the first five time steps in Fig. 9(a), there is a spatially fixed disturbance in the lower part of the FOV. This is a pyrometer, which is required for an accurate measurement of the surface temperature. However, due to the post-processing used in the clustering of the edges as explained in Sec. 2, such disturbances do not deteriorate the edge detection result. Fig. 9(b) shows the estimated angle φ of the plate as a function of the time t. Due to the frame rate of the camera of 30 frames/s, the estimation is performed with a sampling time of $T_s = 1/30\,\mathrm{s}$. As shown in the lower part of this figure, at most 3 iterations of the proposed optimization routine are necessary until the convergence criterion is fulfilled. The estimated spatial position of the plate-fixed coordinate frame is shown in Fig. 9(c). The trajectories from Fig. 9(b) and Fig. 9(c) make sense from a physical point of view because the transitions are adequately smooth and agree well with the movements that can be inferred from looking at Fig. 9(a). Note that the presented approach obviously can handle situations where parts of the plate are outside the FOV.

It takes less than 6 ms to detect the edges within the bitmap and approximately 4 ms to solve the optimization problem in MATLAB (Standard PC with i7-2600 @ 3.4 GHz processor and 16 GB RAM). In the estimation results from Fig. 9, every image captured by the camera was used. Depending on the velocity of the plate, a satisfying estimation result is also achieved if not every captured image is used in the optimization. For the scenario from Fig. 9(a), an increase of the sampling time by a factor of 15 deteriorates the quality of the estimation result only insignificantly.

5. CONCLUSIONS

In this paper, the material tracking problem in heavy-plate rolling was discussed. In particular, the rotation and the position of the plate being maneuvered in front of the mill stand are estimated by means of thermographic images. First, edge pixels are detected in a bitmap captured by an infrared 2D-CCD camera. The information about the plate edges is then utilized in an optimization-based approach to estimate the angular and translational position of the plate. Measurement results of a single plate have shown that the proposed method accurately estimates the position and the orientation of a rolled plate.

Until now, only the measurements of a single plate are available to validate the material tracking approach. However, because of the results obtained for the shown plate and from the gained experience of other vision-based material tracking tasks in hot rolling (cf. Schausberger et al. (2015)) the authors are confident that the proposed method will also lead to satisfying results for plates with different dimensions and material properties.

Further research topics include the automatic rotation of the plate where the presented approach can be used as a measurement to control the roller table and the side guides. Here, feedback control could help to reduce the time needed for the rotation of the plate. That is, the throughput of the rolling process could be increased.

Post-print version of the article: F. Schausberger, A. Steinboeck, A. Kugi, M. Jochum, D. Wild, and T. Kiefer, "Vision-based material tracking in heavy-plate rolling", in *Proceedings of the 17th IFAC Symposium on Control, Optimization and Automation in Mining, Mineral and Metal Processing (MMM)*, vol. 49, Vienna, Austria, 2016, pp. 108–113. DOI: 10.1016/j.ifacol.2016.10.105
The content of this post-print version is identical to the published paper but without the publisher's final layout or copy editing.

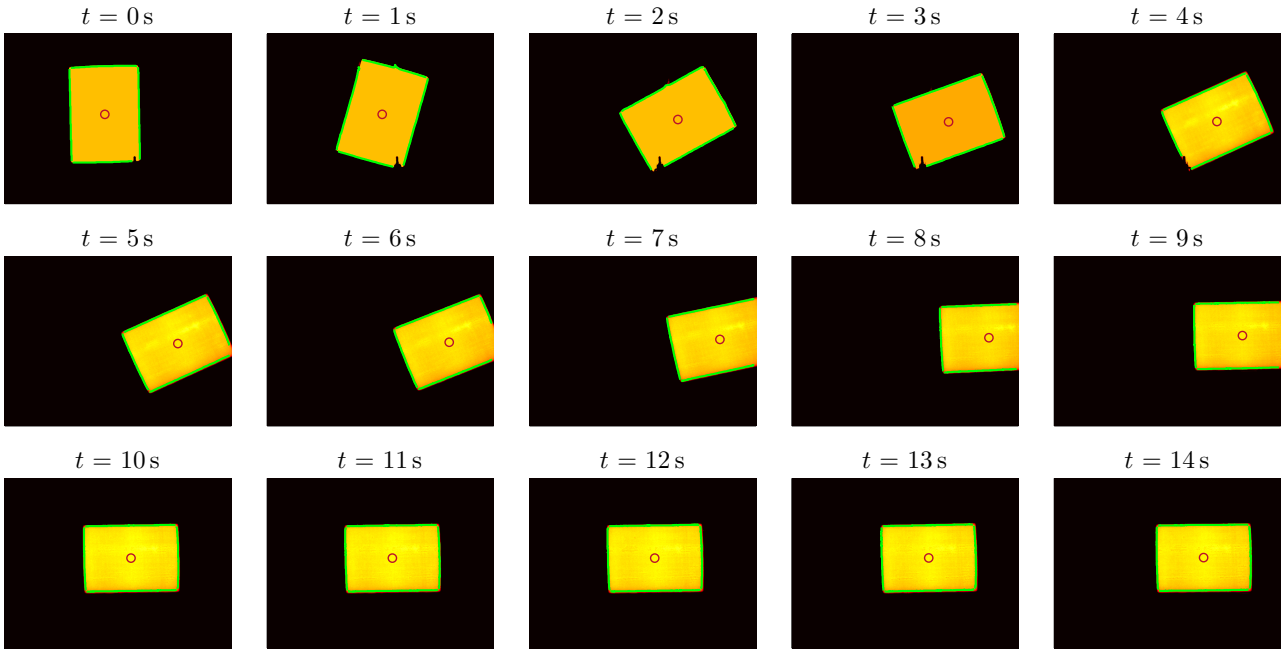

(a) Thermographic images of a plate at different time steps and detected edges. The estimated position of the origin of the plate-fixed coordinate frame $(\Delta x, \Delta y, 0)$ is marked with a red circle.

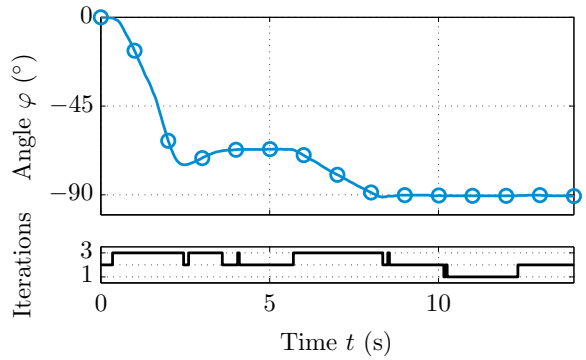

(b) Estimated angle φ of the plate and required optimization iterations. The estimated angles at the time steps shown in Fig. 9(a) are marked with circles.

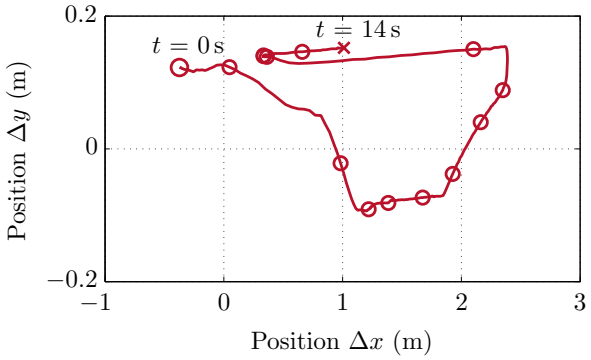

(c) Position $(\Delta x, \Delta y, 0)$ of the plate-fixed coordinate frame. The coordinate frame positions at the time steps shown in Fig. 9(a) are marked with circles.

Fig. 9. Infrared bitmaps and estimation results for a plate rolled at AG der Dillinger Hüttenwerke, Germany.

REFERENCES

Baehr, H.D. and Stephan, K. (2006). *Heat and Mass Transfer*. Springer, New York, 2nd edition.

Canny, J. (1986). A computational approach to edge detection. *IEEE Transactions on Pattern Analysis and Machine Intelligence*, 8, 679–698.

Carruthers-Watt, B.N., Xue, Y., and Morris, A.J. (2010). A vision based system for strip tracking measurement in the finishing train of a hot strip mill. In *Proceedings of 2010 IEEE ICMA*, 1115–1120. Xi'an, China.

González, R.C., Valdés, R., and Cancelas, J.A. (2001). Vision based measurement system to quantify straightness defect in steel sheets. In *Proceedings of 9th International Conference on Computer Analysis of Images and Patterns*, 427–434. Warsaw, Poland.

Montague, R.J., Watton, J., and Brown, K.J. (2005). A machine vision measurement of slab camber in hot strip rolling. *Journal of Materials Processing Technology*, 168, 172–180.

Nocedal, J. and Wright, S.J. (2006). *Numerical Optimization*. Springer Series in Operations Research. Springer, New York.

Orfanidis, S. (1996). *Optimum Signal Processing: An Introduction*. Prentice Hall, New York.

Schausberger, F., Steinboeck, A., and Kugi, A. (2015). Optimization-based estimator for the contour and movement of heavy plates in hot rolling. *Journal of Process Control*, 29, 23–32.

Tratnig, M., Reisinger, J., and Hlobil, H. (2007). A vision-based material tracking system for heavy plate rolling mills. In *Proceedings of IEEE/SPIE 8th International Conference on Quality Control by Artificial Vision (QCAV 2007)*, 1–15. Le Creusot, France.

Post-print version of the article: F. Schausberger, A. Steinboeck, A. Kugi, M. Jochum, D. Wild, and T. Kiefer, "Vision-based material tracking in heavy-plate rolling", in *Proceedings of the 17th IFAC Symposium on Control, Optimization and Automation in Mining, Mineral and Metal Processing (MMM)*, vol. 49, Vienna, Austria, 2016, pp. 108–113. DOI: 10.1016/j.ifacol.2016.10.105